



<http://www.diva-portal.org>

This is the published version of a paper published in *European Physical Journal: Applied physics*.

Citation for the original published paper (version of record):

Esebamen, O X., Thungström, G., Nilsson, H-E., Lundgren, A. (2014)

Comparative Study of UV Radiation Hardness of n+p and p+n Duo-Lateral Position Sensitive Detectors.

European Physical Journal: Applied physics, 68(2): Art. no. 21301

<https://doi.org/10.1051/epjap/2014140253>

Access to the published version may require subscription.

N.B. When citing this work, cite the original published paper.

Permanent link to this version:

<http://urn.kb.se/resolve?urn=urn:nbn:se:miun:diva-22226>

Comparative study of UV radiation hardness of n^+p and p^+n duo-lateral position sensitive detectors

Omeime Xerviar Esebamen^{1,a}, Göran Thungström¹, Hans-Erik Nilsson¹, and Anders Lundgren²

¹ Department of Information Technology and Media, Mid Sweden University, Holmsgatan 10, SE-85170 Sundsvall, Sweden

² SiTek Electro Optics, Ögärdesvägen 13A, SE-43330 Partille, Sweden

Received: 20 June 2014 / Received in final form: 31 July 2014 / Accepted: 12 August 2014
Published online: 15 October 2014 – © EDP Sciences 2014

Abstract. We report experimental results on the degree of radiation damage in two duo-lateral position sensitive detectors (LPSDs) exposed to 193 nm and 253 nm ultraviolet (UV) beam. One of the detectors was an in-house fabricated n^+p LPSD and the other was a commercially available p^+n LPSD. We report that at both wavelengths, the degradation damage from the UV photons absorption caused a much more significant deterioration in responsivity in the p^+n LPSD than in the n^+p LPSD. By employing a simple method, we were able to visualize the radiation damage on the active area of the LPSDs using 3-dimensional graphs. We were also able to characterize the impact of radiation damage on the linearity and position error of the detectors.

1 Introduction

The study of the effect of radiation damage on the electrical properties of radiation detectors is not a new phenomenon [1,2]. The ever increasing interest in the science and engineering of spacefaring and spaceflight signifies that researches in the effect of radiation and radiation damage on detectors will continue for a long time. With the growing demand in applications like photolithography, photoionization, charge-coupled devices (CCDs) and UV photoelectron spectroscopy, detectors with position sensing capabilities that at the same time possess high sensitivity, responsivity and stability are desirable [3].

Numerous studies have in the past and recent times been performed on the stability and performance of numerous detectors under various charge particle irradiation. This range from detectors under electron irradiation [4], X-ray [5], slow-positron and ion beams [6], protons [7], neutron [8] and gamma particles [9]. A number of researches have also been dedicated to the study of position sensitive detectors (PSDs) [10] and the study of radiation and photodetectors for UV applications [11]. Despite these, the subject of PSD linearity under continuous UV radiation has not been extensively explored in scientific literature, hence the theme of this paper.

It is a known fact that a photodetector continuous irradiated with high-energy photons is likely to suffer from responsivity degradation, long-term instability and unreliability [1,2,5]. When ionizing UV photons with high energy travel through the oxide on an oxide-silicon

structure, electron-hole pairs are created. Some electrons are drifted towards the terminals; holes are attracted to the silicon and some electrons and holes recombine. A number of the holes that migrate towards the silicon are trapped in long term trapping sites and a continuous build-up of this process, result in the creation and accumulation of oxide trapped charges and interface states [12]. Over a period of time, these accumulated trapped charges and interface states result in a remanent signal shift that is an indication of radiation damage [12].

Research has shown that the change in the properties of devices like CCDs, MOSFETS and photodiodes arising from UV damage is predominantly as a result of UV-induced effects in the oxide layer and in the Si-SiO₂ interface. These effects comprise of UV-induced absorption in the oxide as a result of color center formation, oxide charges, lattice rearrangement and interfacial modification [13]. As a result, one of the objective of this research was to develop a radiation hard PSD for use under intense medium UV (MUV) environment. The research was performed with UV light beam of 193 nm and 253 nm wavelengths. The fabricated PSD was made and tested alongside a commercially available PSD and a comparison of their position sensing characteristics (linearity and responsivity over the entire surface active area) before and after irradiation is shown.

One challenge often faced by scientists and engineers in the field of radiation detection is locating a particular spot/area on a radiation detector that has been radiation damaged or has undergone a change in responsivity. With CCD devices, it is straightforward by examining the signal collected from each pixel of the device. This is not

^a e-mail: xerviar@yahoo.com

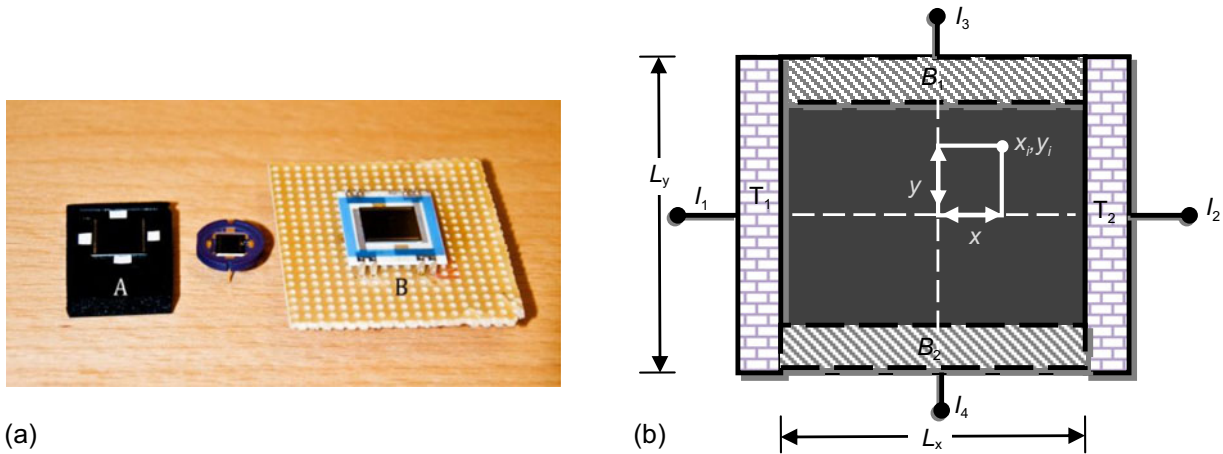


Fig. 1. (a) A line up of three typical LPSDs – two of which were used for this research. Detector A is a commercially available p^+n LPSD from a well known manufacturer of photonic components. Detector B is an n^+p LPSD fabricated in Mid Sweden University. Both detectors are of $10\text{ mm} \times 10\text{ mm}$ dimensions. (b) A schematic of the active area chart of a duo-lateral PSD where I_1 , I_2 , I_3 and I_4 are the current recorded from the four contacts of the LPSD before transimpedance conversion; T_1 , T_2 are the LPSD top contacts and B_1 , B_2 are the orthogonal back/bottom contacts; L_y and L_x are the length and width, respectively, of the detector active area.

the case with PSDs and a host of other radiation detectors. As a result, another objective of this research was to devise a simple method of mapping the response of the active area of a PSD using 3-dimensional graphs. By mapping, one can visualize the distortions, position detection error and change in linearity over the entire surface of the PSD active area caused by radiation damage. The ability to localize or pinpoint a radiation damaged area of a detector means that the unaffected area of a PSD with a radiation damaged spot or section can still be effectively used especially when the effected portion is located at one edge of the active area. The advantage of this mapping method over other techniques like photoelectron emission microscopy traditionally used to image changes at the surface/interface of radiation detectors is that it is much simpler and cost effective because it only involves the use of a beam profiler and simple current-to-voltage converters.

This research is important because a good number of detectors are based on the properties of Si-SiO₂ interface which is very popular in optical radiometry due to the wide availability of silicon, its better temporal stability and high responsivity over a wide (spectral) wavelength. As such, studies on changes in optical properties of silicon detectors from UV radiation can only provide better understanding of the mechanisms responsible for degradation of these detectors and the technology for better radiation hard devices.

2 Theoretical concept

2.1 Duo-lateral position sensitive detector (LPSD)

Position sensitive detectors (PSDs) are optoelectronic position sensors that make use of photodiode surface resistance [14]. One advantage of PSDs over discrete element sensors like CCDs is that the former produces continuous

position signal in one or two axes with high position resolution and high-speed response [15]. A PSD can be a one- or a two-dimensional PSD depending on if it can measure one axis (x or y) or two axes (x and y). Structurally, a two-dimensional PSD can either be a segmented, tetra-lateral or duo-lateral PSD.

Segmented PSDs have common substrates which are segmented into either four separate active areas. Though they are relatively stable and their performance not disturb by temperature change, they are only reliable if the beam overlaps all segments. Tetra-lateral and duo-lateral PSDs are generally referred to as lateral effect PSDs because they are made of a single active element with no gaps or dead zones. These types of detectors determine the position of an ionizing beam by charge sharing via resistive charge division onto sets of two laterally placed readout electrodes. They provide reliable position reading irrespective of the beam size, shape, intensity or profile. This research made use of duo-lateral PSDs because they are renowned for having very small position detection error, excellent linearity over their entire active area as well as can resolve light spot movements of less than 500 nm [16]. Typical examples of duo-lateral PSDs are shown in Figure 1a.

With a duo-lateral PSD, one coordinate (e.g., x coordinate) is measured with two parallel electrodes on top of the device (T_1 , and T_2) as shown in Figures 1b and 2 whereas the other coordinate (y coordinate) is measured with the orthogonally placed electrodes on the backside (B_1 , and B_2). The measured coordinates (x_i , y_i) are derived from a measurement of the resistive charge division in both dimensions and they are mathematically expressed as:

$$x_i = \frac{L_x}{2} \times \frac{I_2 - I_1}{I_2 + I_1}, \quad (1)$$

$$y_i = \frac{L_y}{2} \times \frac{I_4 - I_3}{I_4 + I_3}. \quad (2)$$

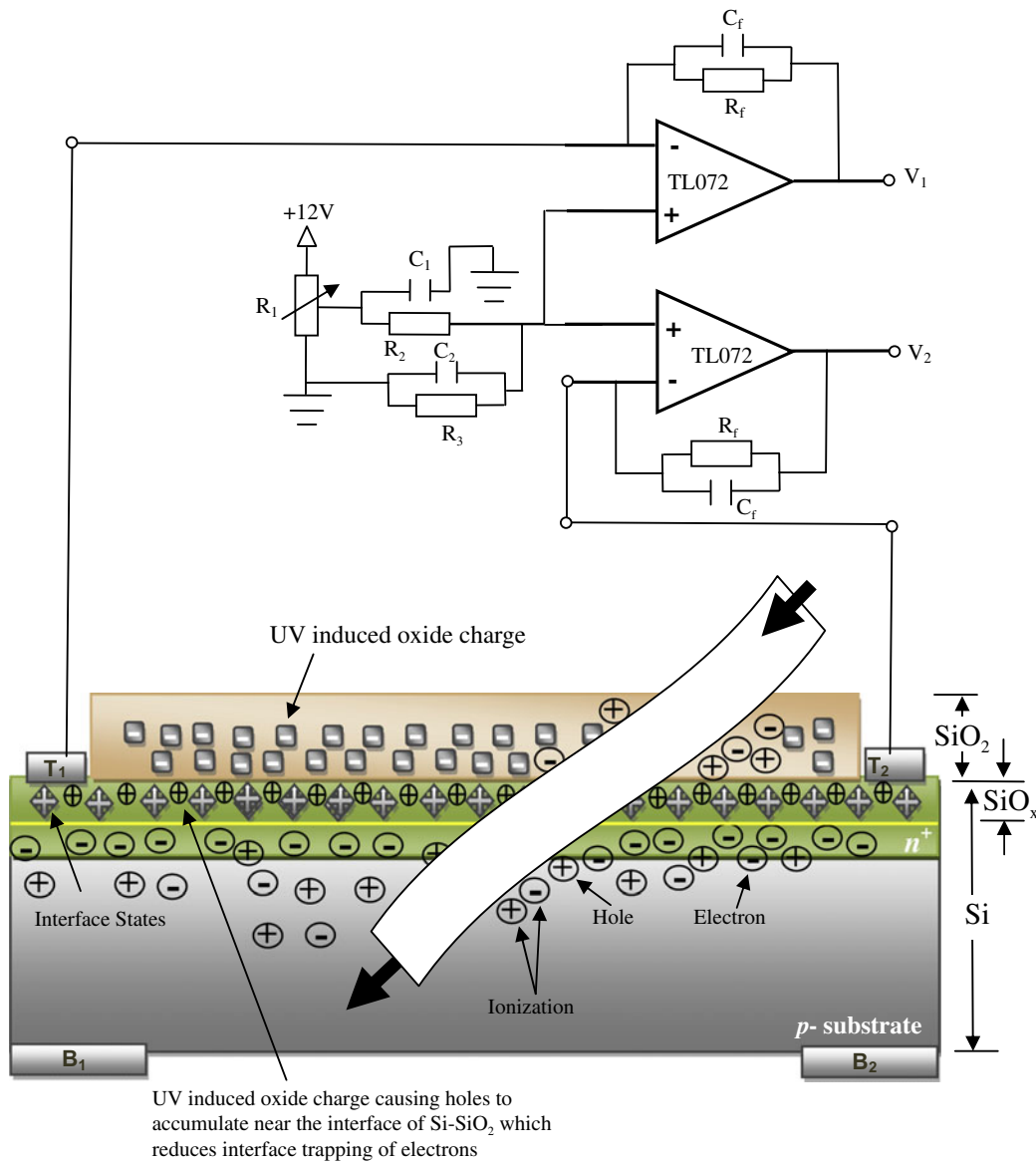


Fig. 2. An illustration (not drawn to scale) of UV induced oxide charges that occur in the vicinity of an interfacial layer (SiO_x) formed between the Si and SiO_2 layers of the detector from the absorption of high energy UV photons. The figure also shows a schematic showing the transimpedance amplification circuit connected to the PSD for current-voltage conversion. The backside contacts B_1 and B_2 are similarly connected just like the front contacts (T_1 and T_2), to a second set of transimpedance amplifiers but biased with -12 V . The feedback capacitors and resistors are labeled as C_f and R_f , respectively.

Although duo-lateral detectors are generally linear, they are still prone to non-linear effects from a number of known and unidentified effects [17]. The eventual deviation on either dimension or axis known as *position non-linearity or error* ε , can be obtained from the difference between the ideal/actual position and the measured position of the beam on the active area [18].

2.2 UV induced oxide charge trappings

As high energy UV beam (with energy $> 9\text{ eV}$; wavelength $< 137\text{ nm}$) travels through the SiO_2 as shown in

Figure 2, some of the incident photons can get absorbed in the SiO_2 layer and electron-hole pairs may be generated in the oxide. A number of the electrons in the valence band gain enough energy to relocate to the conduction band and may drift to the silicon layer to increase the measured quantum efficiency. The probability of structural modifications occurring in the SiO_2 and/or in the Si-SiO₂ interface is increased as more high energy UV photons are absorbed [19]. The lattice arrangement in the oxide and/or silicon is also stressed and rearranged, and changes in the interface properties can occur. As more photons get absorbed in the oxide layer, charge species and negatively charged centers are produced that modify the electrical properties of the device [20].

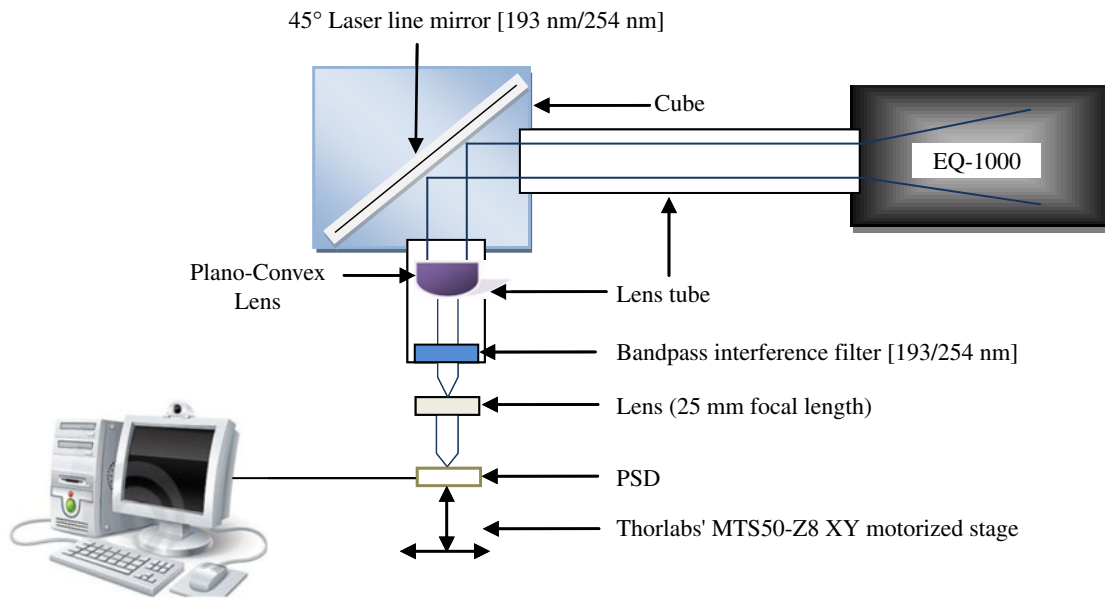


Fig. 3. A schematic of the measurement set-up for the degradation, the 3-dimensions mapping and the linearity measurement of the devices. For the 3-dimensions mapping and the linearity measurement, a $100\ \mu\text{m}$ spot size fiber optic cable and a beam profiler was used in place of the 25 mm focal length lens and bandpass interference filter that were used during the degradation of the PSDs.

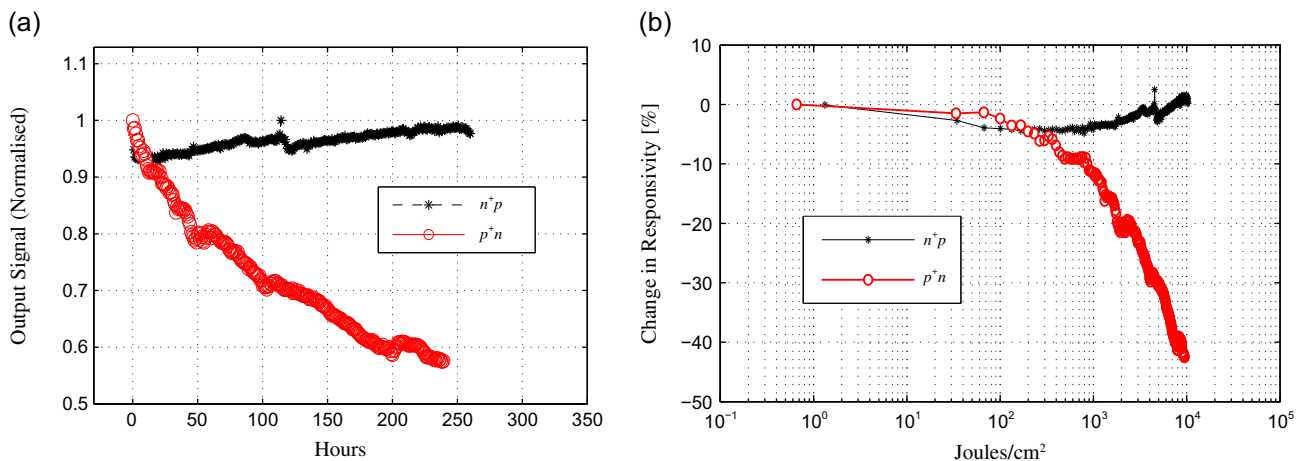


Fig. 4. (a) The photocurrent signal recorded over time from the n^+p and p^+n diodes during irradiation with 193 nm UV photons. (b) Stability of an n^+p compared to p^+n diode when exposed to 193 nm radiation. Both plots are normalized to the initial response.

But with UV beam (wavelength $\gg 137\ \text{nm}$; energy $\ll 9\ \text{eV}$ nm which is less than the bandgap of SiO_2), radiation damage cannot arise from absorption (if any) in the SiO_2 . But instead, damage is due to the increase in the formation of charge centers that also induce a rise in positive charge carriers at the Si-SiO₂ interface. These charges occupy the interface states at the Si-SiO₂ interface and consequently increasing the trappings or recombination of photogenerated electrons. Studies have shown that damage from irradiation of UV beam (with energy $\ll 9\ \text{eV}$; wavelength $\gg 137\ \text{nm}$) on Si-SiO₂ interface structure

could also be due to the build-up of interface traps caused by internal photoemission from Si into SiO₂ [21]. Research has also shown that the fixed oxide charge density at the interface is a function of the accumulative UV dose absorbed [22].

The degree of radiation damage on a device can also be dependent on the doping of the bulk. Studies have shown that for n -type silicon, radiation damage resulting from continuous absorption of charge particles or photons introduces stable defects acting as effective p -type doping whereas, for the p -type silicon, there is no type inversion [23].

3 Device fabrication

The LPSD labeled as “B” in Figure 1a with an active area of 0.0001 m^2 ($10 \text{ mm} \times 10 \text{ mm}$) was fabricated in the cleanroom of Mid Sweden University. It was made from a 100 mm diameter float zone p -silicon substrate with a resistivity of $10 \text{ k}\Omega \text{ cm}$ and $\langle 111 \rangle$ crystal orientation. $0.4 \times 10^{15} \text{ ions/cm}^2$ arsenic ions were implanted at 56 keV through a thin film of SiO_2 mask, Boron ions (dose = $2 \times 10^{14} \text{ ions/cm}^2$) were implanted at 40 keV on the backside to create ohmic contacts and the wafer thereafter annealed at $900 \text{ }^\circ\text{C}$ in nitrogen ambient for a period of 30 min. The depth of the implanted arsenic ions in the substrate was approximately 3000 \AA . A passivation layer of 100 \AA thick SiO_2 film was thermally grown on the top layer and measured using an Avantes AvaSpec-2048 spectrometer. Using electron beam evaporation, 3000 \AA thick aluminium was deposited on the front and backside of the wafer and then followed by patterning of the aluminium layer using a lift-off process to create the electrodes. Forming gas annealing was performed as the final step to limit the density of interface states and process generated traps.

3.1 Pulse conversion and amplification

Since the currents in/out of the electrodes of an LPSD are small and because subsequent analysis took place in the voltage domain, a current to voltage conversion was performed. For this purpose, a transimpedance amplifier was constructed on each electrode with a low noise JFET-input operational amplifier to convert the currents to voltage outputs. The LPSDs were reverse biased through the non-inverting input of the operational amplifier at $\pm 12 \text{ V}$ bias voltage as shown in Figure 2 [24].

3.2 Measurement set up

The detectors were exposed to UV light (193 nm and 253 nm) produced from an Energetiq EQ-1000 laser-driven light source that was part of the experimental setup shown in Figure 3. The experiment was performed in three stages. The first part involved mapping the entire active area and measuring the position deviation and non-linearity of the devices. The next stage was irradiating the detectors over a period of time to cause ionization damage and degradation on the LPSDs under UV beam irradiation. The third part was repeating stage 1 in order to ascertain the induced radiation damage, position deviation and non-linearity of the devices brought about by the degradation. For stages 1 and 3, we used the circuit configuration in Figure 2, a $100 \text{ }\mu\text{m}$ spot size fibre optic cable and an in-house designed beam profiler in place of the 25 mm focal length lens and bandpass interference filter in Figure 3.

During the degradation of the devices in stage 2, they were operated in photodiode photovoltaic mode with the electrodes T_1 and T_2 connected as a common electrode while electrode B_1 and B_2 were connected as another.

For continuous data collection, a programmed Labview data acquisition system was used for stages 1 and 3 while a UDT S370 optometer was used for stage 2.

4 Results

193 nm and 253 nm wavelength exposures were performed with a 0.11 mW/cm^2 and 0.45 mW/cm^2 intensity beam, respectively, to cause ionisation damage on the detectors after a long period of irradiation. As the radiation damage is induced, the output response signal collected from each detector begins to change over time. This is because of the effect of the prolonged irradiation of the photons on the ability of the detectors to efficiently convert absorbed photons into electrical signal.

It is seen from Figure 4a that a 193 nm irradiation of high intensity photons cause an accumulation of high oxide/interface charges and induction of potential traps to significantly reduce the electrical response of detector A (p^+n detector). In the case of detector B (n^+p detector), the recorded output signal steadily rises to a maximum after 250 hours of irradiation before it starts decreasing. After a 100 hours irradiation at 253 nm as seen in Figure 5a, a similar linear decline in signal is observed from the p^+n detector (detector A). At this wavelength, the n^+p detector also shows an increase in current signal over a period of time before it saturates. The increase in signal in the n^+p detector is caused by favourable electron collection and charge multiplication in the LPSD [25]. As more photons are absorbed, the average time it takes for the minority carriers to recombine is increased, thereby reducing the recombination rate of the photogenerated electrons and holes carriers.

A comparison of the stability of both detectors over irradiation time was investigated using the change in responsivity as a function of the intensity as shown in Figures 4b and 5b. It should be noted that the responsivity is the input-output gain of the detector. Specifically, it is a measure of electrical output per UV photon input expressed in Ampere/Watt (A/W).

Under 193 nm photon radiation, the n^+p detector showed a maximum/minimum change in responsivity of $\pm 4\%$ while the p^+n detector showed a drop in responsivity of up to 45% (see Fig. 4b). After the irradiation of 253 nm photons, the n^+p detector only loses 20% of its initial responsivity, while the p^+n detector loses about 62% responsivity. See Figure 5b.

Since the active surface of both detectors comprise of Si-SiO₂ interface, it is imperative to note that the wavelengths used (193 nm i.e., $\sim 6.4 \text{ eV}$; and 253 nm i.e., $\sim 4.9 \text{ eV}$) are below the SiO₂ band gap of 9 eV, and as such, the decrease in the responsivity cannot be attributed to the absorption of photons in the SiO₂ film at the top layer. But instead, it is due to the creation of positive fixed oxide charges and positive or negative interface traps at the trap centers causing a reduction in the mobility of charge carriers. Interface defects, trapping of photogenerated carriers leading to a reduction in quantum efficiency as well as trapped carriers from stressed P_b-hydrogen bonds caused

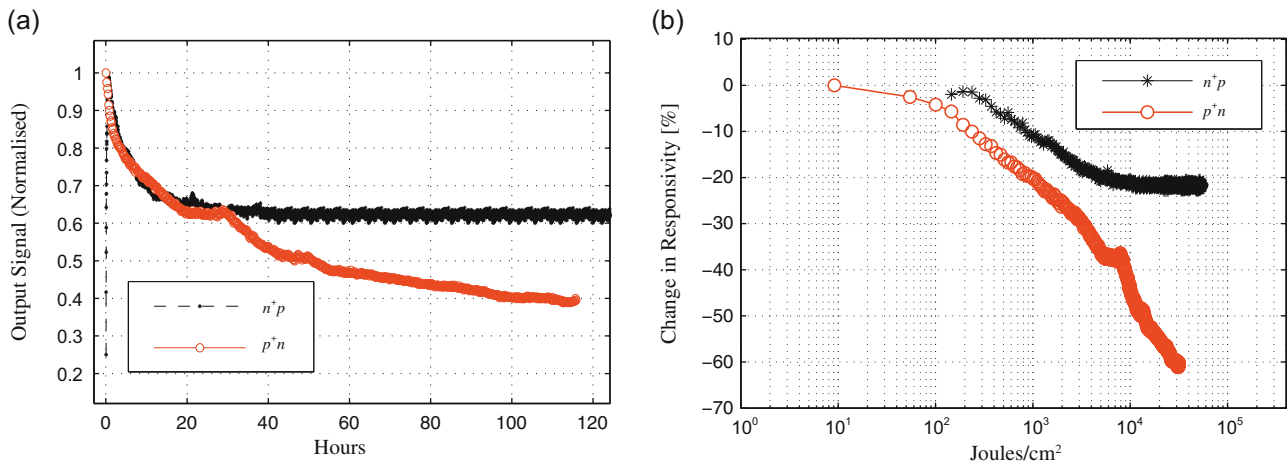


Fig. 5. (a) The photocurrent signal recorded over time from the n^+p and p^+n detectors during irradiation with 253 nm UV photons. (b) The stability of the n^+p LPSD compared to the p^+n LPSD when exposed to 253 nm radiation. Both plots are normalized to the peak response.

by irradiation in the so called P_b centers¹ are other reasons for the degradation of the detector signal [26, 27].

Using the configurations in Figures 2–3 and the principles of an LPSD as described with equation (1), a mapping of the active area of the detectors was done before and after irradiation. With the result, we were able to visualize the localized site of ionization damage and determine the damage impacted on the relative sensitivity and linearity of the LPSD. To demonstrate this, a 4 mm spot size beam with an intensity of 1.4 mW/mm² at 253 nm wavelength was focused on each LPSD for 67 hours. A plot showing the degradation of the devices during the prolonged exposure to pulsed laser is shown in Figure 6a. In order to obtain a very good resolution of the total active area map, a 100 μ m spot size beam was used and several readings similar to Figure 6b were taken with 25 μ m displacement to calculate all x_i, y_i coordinates.

Figure 6b is the output recorded from contacts T_1 and T_2 of the detectors as the beam travel along the y -plane (in the direction of the arrow y in Fig. 6d) and the bump is an indication of the irradiation effect on a location along the beam path.

As expected, the sensitivity over the entire active area of the unirradiated detectors as shown in Figures 6c and 6e are uniform as no degradation has been performed on them. After irradiation, it is seen in Figure 6d that the sensitivity of the irradiated spot described here as the sum of the anode signal, depreciates. While the degradation manifests as an indentation or bump around the irradiated spot in detector A (p^+n detector), the sensitivity across the active area of detector B (n^+p detector) is visibly unaffected as shown in Figure 6f.

To demonstrate how the mapping of the detector surface can be useful in terms of using the unaffected area after a part of an LPSD has been degraded, a second

ionization damage was performed on detector A with the same beam used in the first degradation.

The result can be seen in Figure 6g. With the help of the mapping technique, we were able to locate the area that was previously damaged and then irradiate a new spot even after the detector had been removed from the motorized stage. It is noticed that Figure 6g shows a well formed 4 mm impression of the beam shape because the detector was placed at the precise focal point of the Plano-convex lens. The decrease in sensitivity as a result of degradation was also observed at different wavelength. This was implemented by scanning the p^+n detector using light with a wavelength different from that which degradation was performed and then viewing the degradation from a yz -plane (i.e., relative sensitivity vs PSD length axis). It can be seen that the degradation caused a loss of 80% sensitivity when viewed/scanned using a 253 nm light as can be seen in Figure 6h. But when mapped using a 450 nm beam, a decrease of 20% is observed (Figs. 7a and 7b); and 8% decrease in sensitivity is observed with a 620 nm beam (Figs. 7c and 7d). The true level of degradation is obviously seen in Figures 6g and 6h as it was at this wavelength that the degradation process occurred. The result as expected shows that as the wavelength of the scan beam increases, the true level of degradation reduces. This is because as the beam/light wavelength increases, the penetration or absorption depth in silicon also increases. At 253 nm, the beam is absorbed just below the Si-SiO₂ interface and as a result, the surface defect on silicon arising from irradiation is clearly revealed. Whereas, because at 450 nm and 620 nm the absorption coefficient in silicon before it is absorbed is about 8×10^4 cm⁻¹ and 4×10^3 cm⁻¹, respectively [28], the surface defect showed from the scan is not as evident.

Using the information in Figures 6 and 7, we calculated the induced *position non-linearity* or *error* which is the geometric variation between the actual position and the measured position of incident light spot before and after irradiation of the LPSDs. The error calculated across PSD *width axis* at every 25 μ m step is shown in Figure 8.

¹ P_b centers are trivalent silicon atoms bound to three silicon atoms with an unbound electron in a sp^3 -orbital pointing into the oxide perpendicular to the interface [26].

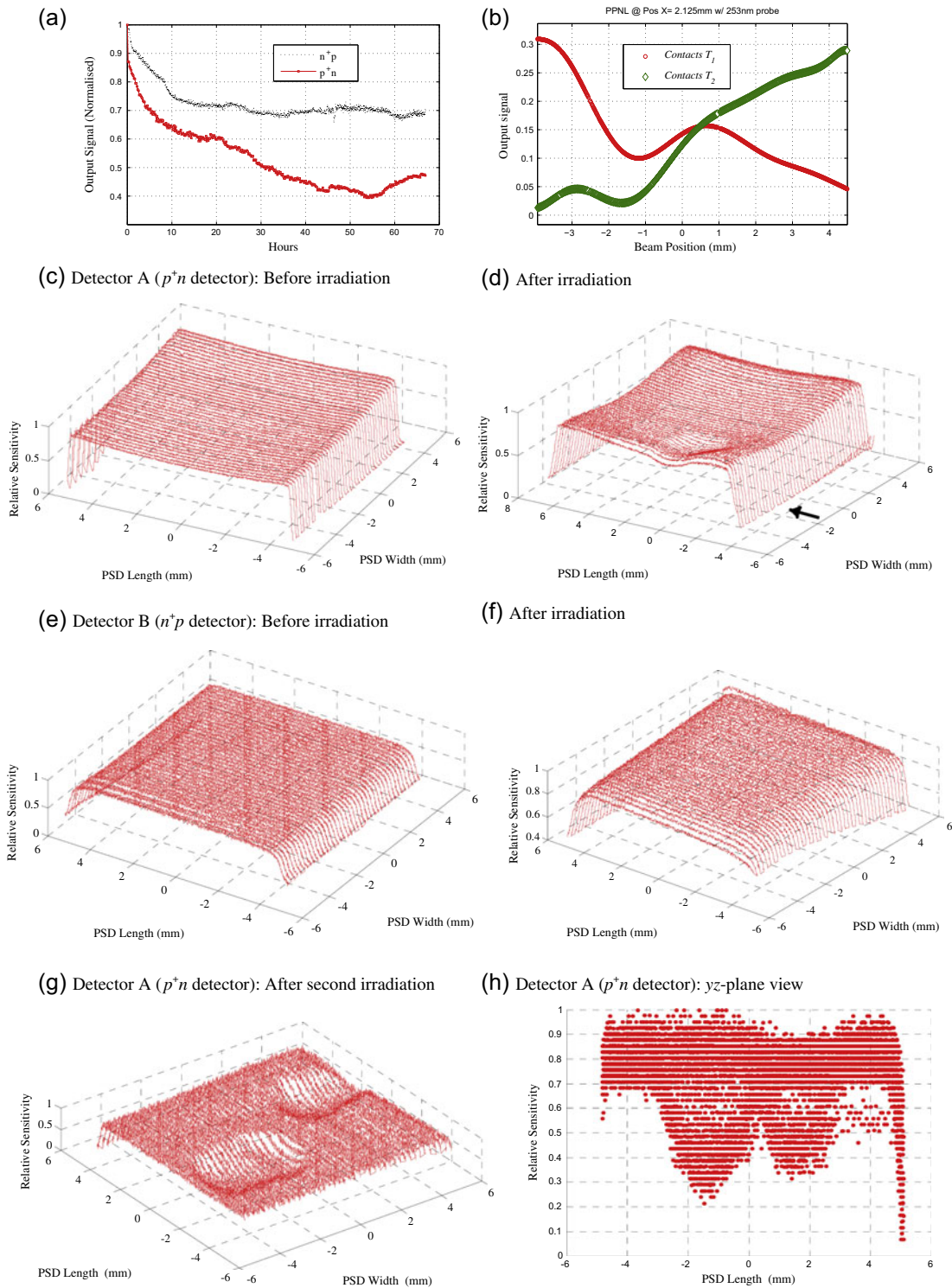


Fig. 6. (a) The response signal of the n^+p and p^+n detectors during degradation with a 1.4 mW/mm^2 , 253 nm UV photons. (b) The recorded output signals of one scan as the beam travel along the y -plane (in the direction of the arrow in Fig. 6d). The signals are as recorded from contacts T_1 and T_2 and the bumps noticed in the signals are indications of the ionization damage effect on the irradiated spot. (c)–(f) are the active area maps of the n^+p and p^+n LPSDs before and after irradiation with 1.4 mW/mm^2 , 253 nm UV photons. It should be noted that the axis labeled as “PSD Width” is a collection of the x -coordinates calculated using equation (1) and the y -coordinates are the “PSD Length” calculated using equation (2). (g) The active area map of the p^+n LPSD after a second degradation process on a previously unaffected region of the detector. (h) The yz -plane view (in the direction across PSD Length axis in Fig. 6g) of the p^+n LPSD showing $\sim 80\%$ loss in sensitivity arising from degradation.

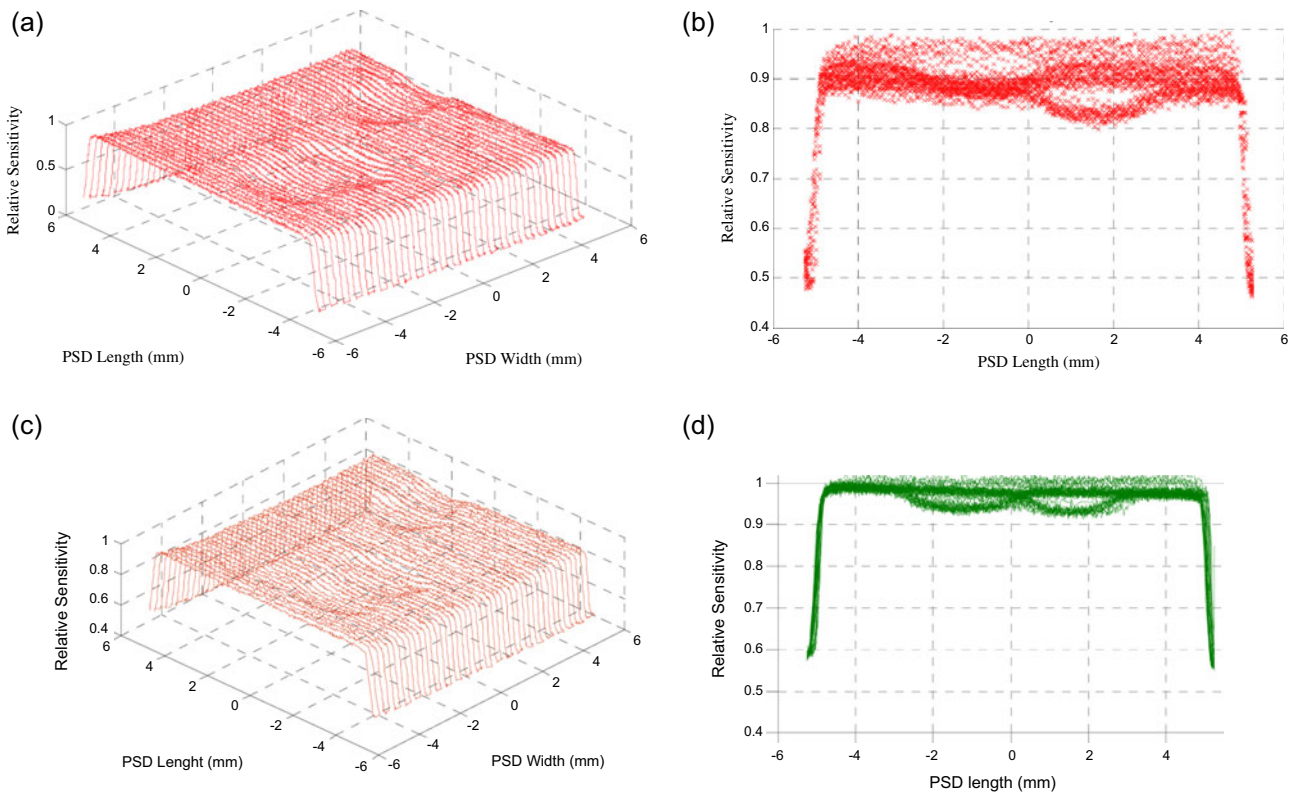


Fig. 7. (a) The degraded active area map of the p^+n LPSD using a 450 nm light through a 100 μm fiber optic cable. (b) The corresponding yz -plane view of the loss in sensitivity arising from degradation. yz -plane is the view in the direction across PSD Length axis in Figure 7a. (c) The degraded active area map of the p^+n LPSD using a 620 nm light. (d) The yz -plane view of the loss in sensitivity arising from degradation as detected using the 620 nm light. The yz -plane is the view in the direction across PSD Length axis in Figure 7c.

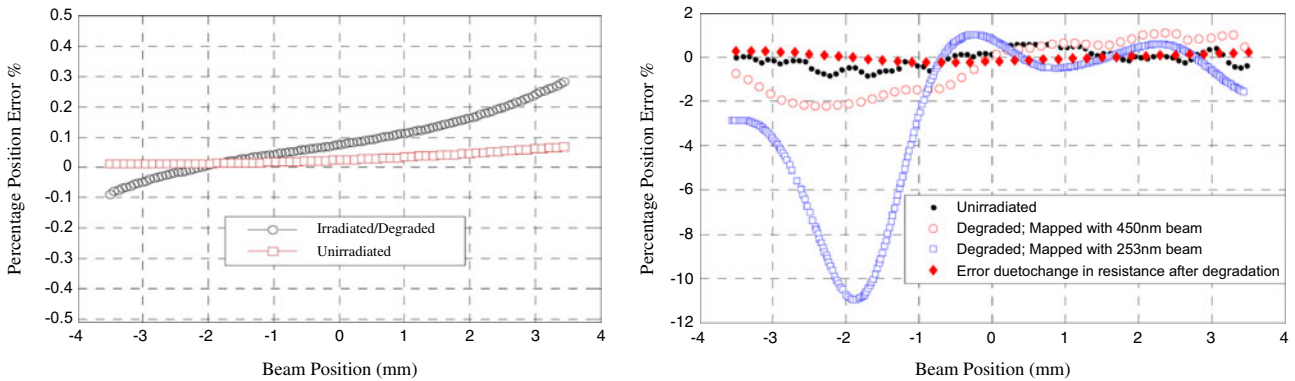


Fig. 8. The percentage error which is the absolute deviation normalized to the detector length measured before and after irradiation of (a) n^+p LPSD. (b) p^+n detector. The position error measured in the unirradiated detectors is due to among other factors, the presence of stray light during measurement and the existence of structural defects and uncertainties inherent in the detectors during device manufacturing [29]. The measured error after irradiation shows that the deviation is further exacerbated by ionization damage.

From Figure 8a, the percentage position error along the measured path or axis is slightly linear and uniform with no visible dent caused by the degradation. As expected, there is a gradual deviation in error recorded prior to degradation with maximum measured error of $\sim 0.1\%$. For the irradiated n^+p detector, there is no visible bump except for the rise in error in comparison with the unirradiated LPSD towards the edge of the active area.

From Figure 8b, the largest error occurs at the area where irradiation was focused on. It can be deduced from the figure that for every 1 μm error present prior to degradation, there is deflection in spatial non-linearity (~ 4 times worse off when mapped at 450 nm; and ~ 17 times when mapped at 253 nm) at the spot with most damage after degradation in the p^+n detector. This indicates that, damage induced from the effect of UV ionization will create a

major shift in the geometric variation between the actual position and the measured position of incident light spot. The non-appearance of a visible dent in the sensitivity or percentage error of the irradiated n^+p detector is an indication that a significantly higher intensity of 253 nm UV light is required to create the kind of damage noticed on the p^+n detector. It is also a proof that the irradiated n^+p detector is not overly affected by the dominant electron trapping caused by the displacement damage defect of the UV beam. The n^+p detector is more radiation resistant because it has lesser concentration of holes at the interface that can result in interface traps and also as there is no introduction of stable defects from radiation in the p -type substrate which can result in type inversion unlike the p^+n LPSD (fabricated on the n -type substrate).

5 Conclusion

We have reported results on the radiation damage caused on two lateral position sensitive detectors using 193 and 253 nm ultraviolet radiations. One of the detectors was an in-house fabricated n^+p LPSD and the other was a commercially available p^+n LPSD. At both wavelengths, the degradation damage as a result of the UV photons caused a much more significant deterioration of responsivity in the p^+n LPSD compared to the n^+p LPSD. By using a very narrow beam, a transimpedance circuit and a beam profiler, we were able to visualize the radiation damage on the active area of the LPSDs with 3-dimensional graphs. The merit of this method is that it is much simpler and cost effective than other methods like photoelectron emission microscopy traditionally used to image changes at the surface/interface of radiation detectors. By using this novel mapping technique, it was possible to map the signal response of the entire active area and to image the part that has suffered any loss in sensitivity and responsivity. By applying this method, we were also able to calculate the effect of radiation damage on the linearity and position error of the detectors. The results show that prolonged UV radiation has a significant negative impact on the linearity and as such increases the position deviation of the detectors. The results also show that the n^+p LPSD is more UV radiation hard than the p^+n LPSD.

References

1. H.M. Mann, J.L. Yntema, IEEE Trans. Nucl. Sci. **11**, 201 (1964)
2. G. Dearnaley, IEEE Trans. Nucl. Sci. **10**, 106 (1963)
3. M. Tian, J. Mi, J. Shi, N. Wei, L. Zhan, W. Huang, Z. Zuo, C. Wang, X. Luo, Optoelectron. Lett. **10**, 24 (2014)
4. R. Radu, E. Fretwurst, R. Klanner, G. Lindstroem, I. Pintilie, Nucl. Instrum. Methods Phys. Res.: A Accel. Spectrom. Detect. Assoc. Equip. **730**, 84 (2013)
5. J. Zhang, E. Fretwurst, R. Klanner, H. Perrey, I. Pintilie, T. Poehlsen, J. Schwandt, J. Instrum. **6**, C11013 (2011)
6. A. Kinomura, R. Suzuki, T. Ohdaira, N. Oshima, B.E. O'Rourke, T. Nishijima, J. Phys.: Conf. Ser. **443**, 012043 (2013)
7. E. Auffray, A. Barysevich, A. Fedorov, M. Korjik, M. Koschan, M. Lucchini, V. Mechinski, C.L. Melcher, A. Voitovich, Nucl. Instrum. Methods Phys. Res.: A Accel. Spectrom. Detect. Assoc. Equip. **721**, 76 (2013)
8. R. Korde, A. Ojha, R. Braasch, T.C. English, IEEE Trans. Nucl. Sci. **36**, 2169 (1989)
9. L. Xu, W. Jie, G. Zha, Y. Xu, X. Zhao, T. Feng, L. Luo, W. Zhang, R. Nan, T. Wang, CrystEngComm. **15**, 10304 (2013)
10. T. Doke, J. Kikuchi, H. Yamaguchi, S. Yamaguchi, K. Yamamura, Nucl. Instrum. Methods Phys. Res.: A Accel. Spectrom. Detect. Assoc. Equip. **261**, 605 (1987)
11. E. Borch, R. Macii, M. Bruzzi, M. Scaringella, Nucl. Instrum. Methods Phys. Res.: A Accel. Spectrom. Detect. Assoc. Equip. **658**, 121 (2011)
12. T. Oldham, *Ionizing Radiation Effects in MOS Oxides* (World Scientific, New Jersey, USA, 2000)
13. F.M. Li, O. Nixon, A. Nathan, IEEE Trans. Electron Devices **51**, 2229 (2004)
14. H. Andersson, G. Thungström, A. Lundgren, H.-E. Nilsson, Nucl. Instrum. Methods Phys. Res.: A Accel. Spectrom. Detect. Assoc. Equip. **531**, 140 (2004)
15. Hamamatsu, *Hamamatsu Document library*, 2010. [Online]. Available: http://www.hamamatsu.com/resources/pdf/ssd/psd_techinfo_e.pdf [Accessed: 10-Feb-2014]
16. G.P. Petersson, L.-E. Lindholm, IEEE J. Solid-State Circuits **13**, 392 (1978)
17. H.A. Andersson, C.G. Mattsson, G. Thungström, A. Lundgren, H.-E. Nilsson, Nucl. Instrum. Methods Phys. Res.: A Accel. Spectrom. Detect. Assoc. Equip. **563**, 150 (2006)
18. W. Wang, I.J. Busch-Vishniac, IEEE Trans. Electron Devices **36**, 2475 (1989)
19. H. Flicker, J. Loferski, J. Scott-Monck, Phys. Rev. **128**, 2557 (1962)
20. Y.F. Lu, W.K. Choi, Y. Aoyagi, A. Kinomura, K. Fujii, J. Appl. Phys. **80**, 7052 (1996)
21. G.D. Wilk, R.M. Wallace, J.M. Anthony, J. Appl. Phys. **89**, 5243 (2001)
22. C. Fiori, R.A.B. Devine, P. Meiland, J. Appl. Phys. **58**, 1058 (1985)
23. G. Casse, P.P. Allport, M. Hanlon, Improving the radiation hardness properties of silicon detectors using oxygenated n-type and p-type silicon, in *1999 Fifth European Conference on Radiation and Its Effects on Components and Systems, RADECS 99 (Cat. No. 99TH8471, Abbaye de Fontevraud, France)*, pp. 114–119
24. O.X. Esebamen, H.-E. Nilsson, G. Thungström, A. Lundgren, IET Optoelectron. (2014), DOI: 10.1049/iet-opt.2014.0002
25. M. Moll, Recent advances in the development of radiation tolerant silicon detectors for the super-Lhc, in *Astroparticle, Particle and Space Physics, Detectors and Medical Physics Applications – Proceedings of the 11th Conference, Villa Olmo, Como, Italy, 2010*, pp. 101–110
26. K.L. Brower, Phys. Rev. B **38**, 9657 (1988)
27. S.K. Lai, J. Appl. Phys. **54**, 2540 (1983)
28. M.A. Green, M.J. Keevers, Prog. Photovolt. Res. Appl. **3**, 189 (1995)
29. H. Nakajima, K. Sumi, H. Inujima, IEEE Trans. Instrum. Meas. **59**, 3041 (2010)